Journal of Power Sources 246 (2014) 260–268

Contents lists available at ScienceDirect

Journal of Power Sources

journal homepage: www.elsevier.com/locate/jpowsour

Poly(ethylene glycol) grafted multi-walled carbon nanotubes/$LiFePO_4$ composite cathodes for lithium ion batteries

Chunli Gong [a,b], Zhigang Xue [a,*], Xiaoen Wang [a], Xing-Ping Zhou [a], Xiao-Lin Xie [a,*], Yiu-Wing Mai [c]

[a] Key Laboratory for Large-Format Battery Materials and Systems, Ministry of Education, School of Chemistry and Chemical Engineering, Huazhong University of Science and Technology, Wuhan 430074, China
[b] Faculty of Chemistry and Material Science, Hubei Engineering University, Xiaogan 432100, Hubei, China
[c] Centre for Advanced Materials Technology (CAMT), School of Aerospace, Mechanical and Mechatronic Engineering J07, The University of Sydney, Sydney, NSW 2006, Australia

HIGHLIGHTS

- We report a new conductive agent to increase the electrochemical property of $LiFePO_4$.
- PEG layer improves the dispersion of MWCNTs and facilitates Li^+ diffusion in the cathode.
- Highly dispersed MWCNTs increase the thermal conductivity of the cathode.

GRAPHICAL ABSTRACT

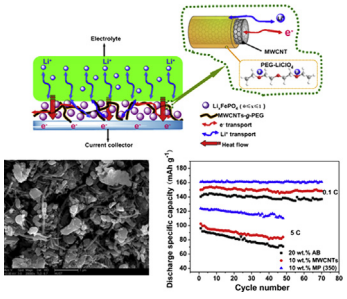

ARTICLE INFO

Article history:
Received 17 May 2013
Received in revised form
9 July 2013
Accepted 26 July 2013
Available online 2 August 2013

Keywords:
Lithium iron phosphate
Carbon nanotube
Poly(ethylene glycol)
Composite cathode
Lithium ion battery

ABSTRACT

Poly(ethylene glycol) (PEG) grafted multi-walled carbon nanotubes (MWCNTs-*g*-PEG or MP) were synthesized and used to modify $LiFePO_4$ as cathodes for lithium-ion batteries (LIBs). The effects of different molecular weights of PEG grafted on MWCNTs and different mass fractions of MP on the properties of $LiFePO_4$/MP composite cathodes were evaluated by their morphology, charge–discharge tests, electrochemical impedance spectroscopy, electrical and thermal conductivities. Their electrochemical behaviors at ambient temperature and low temperature, high rate capability and cycling performance were observed in the presence of the MP additives. The lithium ions diffusion in the $LiFePO_4$/MP composite electrodes was almost 2 orders of magnitude higher than that in the $LiFePO_4$/acetylene black (AB) electrode when the conductive additive content was 5 wt.%. Thermal studies of $LiFePO_4$/MP were also examined by the heat-pole method, which showed higher thermal conductivity of the cathode in cases of MP being incorporated into $LiFePO_4$ particles than $LiFePO_4$ cathodes with AB or MWCNTs additives. These results suggest that MP is a promising conductive additive to increase the electrochemical performances, thermal transport and safety of $LiFePO_4$ cathodes for LIBs.

1. Introduction

With rising interest in the commercialization of hybrid electric vehicles (HEVs) and electric vehicles (EVs) for the automotive industry, there has been much increasing attention on the

* Corresponding authors. Tel.: +86 27 87793241; fax: +86 27 87543632.
E-mail addresses: zgxue@mail.hust.edu.cn (Z. Xue), xlxie@mail.hust.edu.cn (X.-L. Xie).

0378-7753/$ – see front matter © 2013 Elsevier B.V. All rights reserved.
http://dx.doi.org/10.1016/j.jpowsour.2013.07.091

development of improved lithium-ion batteries (LIBs) [1]. For large-scale applications such as power supplies, electrode materials in LIBs must possess higher electrical/ionic conductivity, higher safety and lower cost than those currently achieved. The olivine-type $LiFePO_4$, which is representative of current cathode materials, has developed rapidly since it was first used as cathode materials by Goodenough et al. [2,3]. It is shown that a phase-separation reaction occurs in the lithium insertion/extraction process in the $LiFePO_4$–$FePO_4$ system [2], and the theoretical specific capacity is 170 mAh g^{-1} at a high and flat operating voltage of around 3.45 V versus Li^+/Li, which is well within the electrochemical stability window of the non-aqueous Li-based electrolytes [4]. Besides, $LiFePO_4$ has attracted particular attention owing to its high safety associated with the strong covalent P–O bonds in the PO_4^{3-} poly-anionic clusters, high thermal stability even in the over-charged state, low cost and low toxicity [5]. However, it is difficult to reach the full theoretical capacity in a $LiFePO_4$ cathode caused by its poor intrinsic electronic conductivity ($\sim 10^{-9}$ S cm^{-1}) [6] and low lithium ion diffusion coefficient, bringing obstacles for practical applications in high-rate batteries.

Many efforts have been made to overcome the above drawbacks by coating or depositing the $LiFePO_4$ particles with an electronic-conductive layer [7–9], doping the olivine structure with cations [10], reducing the $LiFePO_4$ particle size [11] and fabricating porous structures [12]. Among these reported methods, carbon coating is a very efficient way to resolve the issue of limited rate capacity caused by the extremely low electrical conductivity of $LiFePO_4$, and the electrochemical performances are thus improved in the presence of dispersed carbon particles which provide pathways for electron transfer [4]. Also, the incorporation of highly conducting carbon materials into $LiFePO_4$ has been proven an effective strategy to enhance conductivity of $LiFePO_4$-based electrodes. To-date, various forms of carbon materials, such as acetylene black (AB) [2], carbon black [13], conductive graphite [14], one-dimensional (1D) carbon nanotubes (CNTs) [15–17] or carbon fibers [18] and two-dimensional (2D) graphenes [5,19,20] have been used as conductive additives in the cathode system. Besides the formation of a conducting network by bridging the active particles with these carbon-based additives, the structures and shapes of carbonaceous materials and their dispersion in the active materials play important roles in determining the electrochemical performance of the cathode materials.

Compared with conventional conductive additives, CNTs appear promising to improve the electrochemical properties of different cathode materials due to their 1D geometry, extremely high aspect ratio and superior electrical conductivity [21]. Further, the exceptional mechanical properties of CNTs [22,23] can reduce the residual stresses caused by volume changes in the electrode materials [24,25]. It is noted that the excellent thermal conductivity of individual multi-walled carbon nanotubes (MWCNTs) (3000 W m^{-1} K^{-1}) [26], surpasses the graphite ($\sim$300 W m^{-1} K^{-1}) and carbon black ($<$1 W m^{-1} K^{-1}) [27]. This is beneficial to the thermal runaway caused by over-charge or high current charge–discharge, and the high safety of the LIBs system is guaranteed. Toprakci et al. [16] and Sun et al. [17] reported the improved specific capacities and rate performances based on $LiFePO_4$ and MWCNTs or single-walled carbon nanotubes (SWCNTs) composite cathodes. However, the dispersion of CNTs in solvents is quite difficult owing to their high van der Waals forces between CNTs through large surface area [24,28], which limits the formation of an effective conducting network in the electrode. The developments of dispersion of CNTs and other carbon materials have become a challenge to improve the performance of CNTs used as additives in electrode materials. However, CNTs are just a pure electrical conductor, which cannot fundamentally solve the problem of slow transportation of lithium ions in the solid electrodes. Kim and co-workers [24] very recently prepared $LiNi_{1/3}Co_{1/3}Mn_{1/3}O_2$ cathodes containing different functionalized MWCNTs, such as acid treatment, amino functionalization and silanization. It is found that silane-functionalized MWCNTs can significantly reduce the electrical resistance and improve the electrochemical performance of the nanocomposite cathodes due to their superb dispersion state in the active particles. In addition, poly (ethylene glycol) (PEG) is usually used to functionalize CNTs to improve its dispersion in solvents [29,30]. Moreover, PEG is a very good solvent for lithium salts and becomes the first and the most widely studied polymer electrolyte matrix [31–33]. Notwithstanding CNTs have been used as additives in cathode materials, the simultaneous increases of electrical and ionic conductivities by the incorporation of functionalized CNTs are rarely studied in $LiFePO_4$-based composite cathodes. Meanwhile, only a few reports [27,34,35] have investigated the thermal conductivity and the potential safety improvement of the cathode composites based on CNTs additives for LIBs.

Herein, we prepared PEG grafted MWCNTs system (MWCNTs-*g*-PEG or simply MP) using low cost raw materials and then used MP as conductive additives in $LiFePO_4$-based cathodes. Not only do the PEG grafted on MWCNTs serve to improve the dispersion of MWCNTs in the active particles they also enhance lithium ions diffusion in the electrodes (Scheme 1). Thus, the electrochemical performance of cathode materials for LIBs is improved. The effects of different molecular weights of PEG grafted on MWCNTs and different mass fraction of MP on morphology and electrochemical properties of $LiFePO_4$-based cathodes are evaluated. The improved discharge capacities at low temperature and thermal management capabilities are also investigated.

2. Experimental

2.1. Materials

MWCNTs (purity >95 wt.%, with an average diameter of 50 nm and length ranging between 5 and 15 μm) were purchased from Shenzhen Nanotech Port Co. Ltd., China. Poly(ethylene glycol) monomethyl ethers (HO-mPEG-OMe, M_w = 350 and 1000), purchased from Aladdin reagent Inc., were dehydrated by azeotropic treatment in toluene before use. *N*,*N*-dimethylformamide (DMF), tetrahydrofuran (THF), toluene, and acetonitrile (MeCN) were distilled and kept in 4 Å molecular sieves to eliminate any traces of water. $LiClO_4$ (Sinopharm Chemical Reagent Co., Ltd) was dried under high vacuum at 130 °C for 24 h before use. Thionyl chloride ($SOCl_2$), concentrated HNO_3 and H_2SO_4 and all other solvents were used directly without any further purification. Commercial battery-grade, carbon coated (C-coated) $LiFePO_4$ powders (2.05 wt.% of C content) were supplied by Shenzhen Kejingstar Technology Ltd., China.

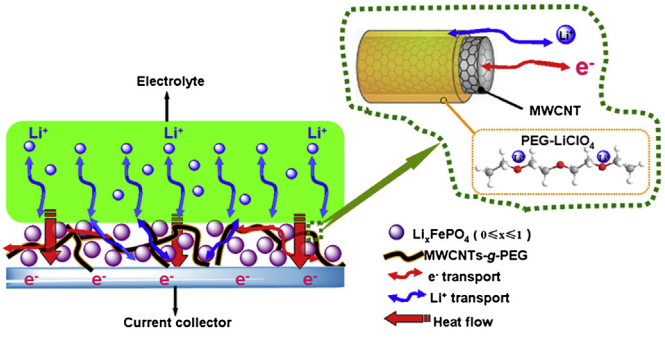

Scheme 1. Schematic illustration for the transport of electrons, lithium ions and heat flow in the LFP/MP based cathode.

2.2. Preparation of MWCNTs-g-PEG

MWCNTs-*g*-PEG (MP) was synthesized using an esterification method (see Fig. S1 in the Supplementary materials) as described in Refs. [29,36]. Typically, pristine MWCNTs were ultrasonically dispersed in a mixture of concentrated HNO_3/H_2SO_4 (1:3 v/v) at ambient temperature for 2 h, followed by magnetic stirring at 60 °C for 6 h to prepare carboxylic acid functionalized MWCNTs (MWCNTs-COOH), which was sonicated in DMF for 0.5 h to give a homogeneous suspension. The as-prepared MWCNTs-COOH solution was subsequently reacted with excess neat $SOCl_2$ at 80 °C for 24 h under Ar atmosphere. The obtained mixture was vacuum-filtered through a polytetrafluoroethylene (PTFE) membrane (0.22 μm) and the desired filter residues were washed with anhydrous THF until the filtrate became colorless. The black solid collected on the membrane was dried under vacuum to give the acyl chloride-functionalized MWCNTs (MWCNTs-COCl) which, in turn, was dispersed in DMF, followed by adding HO-mPEG-OMe to the mixture and kept magnetic stirring at 120 °C for 48 h under Ar atmosphere. After cooling to ambient temperature, the raw solids were separated from the mixture by filtration with a polyvinylidene fluoride (PVDF) membrane (0.22 μm) and washed thoroughly with ethanol and deionized water. The resulting MP was obtained by drying the black solid on the membrane. Two different PEG (with $M_w = 350$ and 1000) grafted MWCNTs were denoted MP-350 and MP-1000, respectively.

MP/$LiClO_4$ complex was prepared by blending the MP and $LiClO_4$ in anhydrous MeCN at ambient temperature for 5 h under Ar atmosphere. The molar ratio of grafted-PEG to $LiClO_4$ was kept constant corresponding to 8 mol of ethylene oxide for 1 mol of Li^+. The MP/$LiClO_4$ powder was obtained after evaporating the solvent from the above suspension at 100 °C under vacuum.

2.3. Characterization

The carbon content in the carbon coated $LiFePO_4$ powders was determined by elemental analysis (Vario EL II, Germany) and thermal gravimetric analysis (TGA, Perkin Elmer Co., USA). The chemical structure of MP was analyzed by Fourier transform infrared spectroscopy and Raman spectra by using a VERTEX 70/FRA 106 Fourier's Infrared/Raman Spectrometer (Bruker Inc., Germany). X-ray photoelectron spectroscopy (XPS) measurement was recorded on a VG MultiLab 2000 (Thermo Electron Co., USA) spectrometer using a monochromatized AlK_α X-ray source. TGA was also conducted on the PE TGA-7 instrument at a heating rate of 10 °C min^{-1} in an argon flow to determine the content of the grafted-PEG. The morphology and size of the MP were also observed by scanning electron microscopy (SEM, FEI Co., Netherlands) and transmission electron microscopy (TEM, FEI Co., Netherlands) at an accelerating voltage of 200 kV. Before TEM examination, the samples were ultrasonically treated in ethanol and then deposited on 200-mesh C-coated copper grids. The phase identification of the samples was conducted with an X-ray diffractometer (XRD, X'Pert PRO, PANalytical B.V.) using CuK_α radiation in the 2θ range 10°–80°.

2.4. Electrochemical measurements

The cathode film was prepared by mixing active materials ($LiFePO_4$), conductive additives, and PTFE binder in pure isopropyl alcohol to form a paste. The amount of binder PTFE was fixed at 5 wt.% and the weight ratio of $LiFePO_4$ to conductive additive was $(95 - x) : x$ (where $x = 3, 5, 8, 10, 15$ and 20). After rolling to a thin film of ~150 μm in thickness, it was cut into circular discs. This circular film was pressed to a stainless steel mesh with a pressure of 10 MPa to fabricate the cathode. The resulting $LiFePO_4$-based cathodes with acetylene black (AB), MWCNTs and MP as conductive additives were denoted as LFP/AB, LFP/MWCNTs and LFP/MP, respectively. These film-type electrodes were assembled into CR2016 coin-type cells with lithium metal as a counter electrode, 1 M $LiPF_6$ in ethylene carbonate (EC)/diethyl carbonate (DEC) (1:1, v/v) as electrolyte, and a Celgard 2400 as separator in an argon-filled glove box. The assembled cells were charged and discharged under different current densities within the voltage range 2.5–4.2 V (vs. Li^+/Li) using a CT2001A cell test instrument (LAND Electronic Co., China). The specific capacities of the samples were calculated based on the mass of the $LiFePO_4$. The electrochemical impedance spectroscopy (EIS) measurements were performed on an electrochemical workstation (Autolab PGSTAT302N, Switzerland) in the frequency range 100 kHz–0.01 Hz with amplitude of 5 mV. Cyclic voltammetry (CV) was conducted between 2.5 V and 4.2 V at 0.1 mV s^{-1} using a CS350 electrochemical workstation. Electrical conductivities of these cathode films were measured by the four-point DC method using the S-2A probe station equipped with an Agilent 34401A ammeter and a Keithley 2400 voltmeter. Thermal conductivities were conducted on a QTM-500 quick thermal conductivity meter (Kyoto Electronics Manufacturing Co. Ltd., Japan) according to the Chinese Standard GB/T-10297-98. All the above tests were carried out at ambient temperature unless indicated otherwise.

3. Results and discussion

3.1. Characterization of MWCNTs-g-PEG

The MP was characterized by FTIR, XPS, Raman spectroscopy, TEM, and TGA. Evidence for covalent functionalization of the side wall of MWCNTs after esterification reaction can be determined by FTIR analysis. As shown in Fig. 1a, the spectrum of the MWCNTs-COOH shows a very weak peak at ~1720 cm^{-1} assigned to the carbonyl stretch of the carboxylic acid group [37]. Since the MWCNTs can absorb infrared rays, the hydroxyl stretching vibration is so weak that it does not appear. New characteristic bands occur after the grafting reaction. The sp^3 C–H stretching absorptions that arise from the alkyl chain appear at ~2930 and ~2850 cm^{-1}. The peaks located at 1070 and 1740 cm^{-1} can be assigned to the vibrations of C–O–C and the carbonyl of the ester, respectively, indicative of chemical grafting of PEG. Raman spectra also support successful modification of MWCNTs with PEG. The Raman spectrum of the purified MWCNTs exhibits a tangential mode (G band) at 1600 cm^{-1} and a disordered mode at 1300 cm^{-1} (D band) that probably arises from defects formed during either synthesis or purification of the nanotubes. After functionalization, the D band appeared to be enhanced significantly for the MP compared to the pristine MWCNTs (Fig. 1b). As the D band is the diagnostic of the disruption in the graphitic layer of MWCNTs, the increase of the relative intensity of this band provided the direct evidence of covalent modification.

X-ray photoelectron spectroscopy (XPS) can be used to determine the surface composition and the functional groups on the MWCNTs. The XPS survey of pristine MWCNTs (Fig. 1c) shows a strong C 1s peak at 284.5 eV and a very weak O 1s peak at 532.6 eV, possibly caused by physically adsorbed oxygen to the surface of the carbon tubes [38]. After acidification, a relatively strong O 1s peak appears with an atom ratio of oxygen to carbon (O/C) as 0.115. Compared to that for the MWCNTs-COOH, the O 1s peaks in MP-350 and MP-1000 become evidently stronger, which is attributed to the grafted PEG chains [39]. The O/C atom ratio is increased to 0.181 and 0.191 for MP-350 and MP-1000 systems, respectively. High resolution C 1s spectra of MWCNTs-COOH (Fig. S2a), MP-350

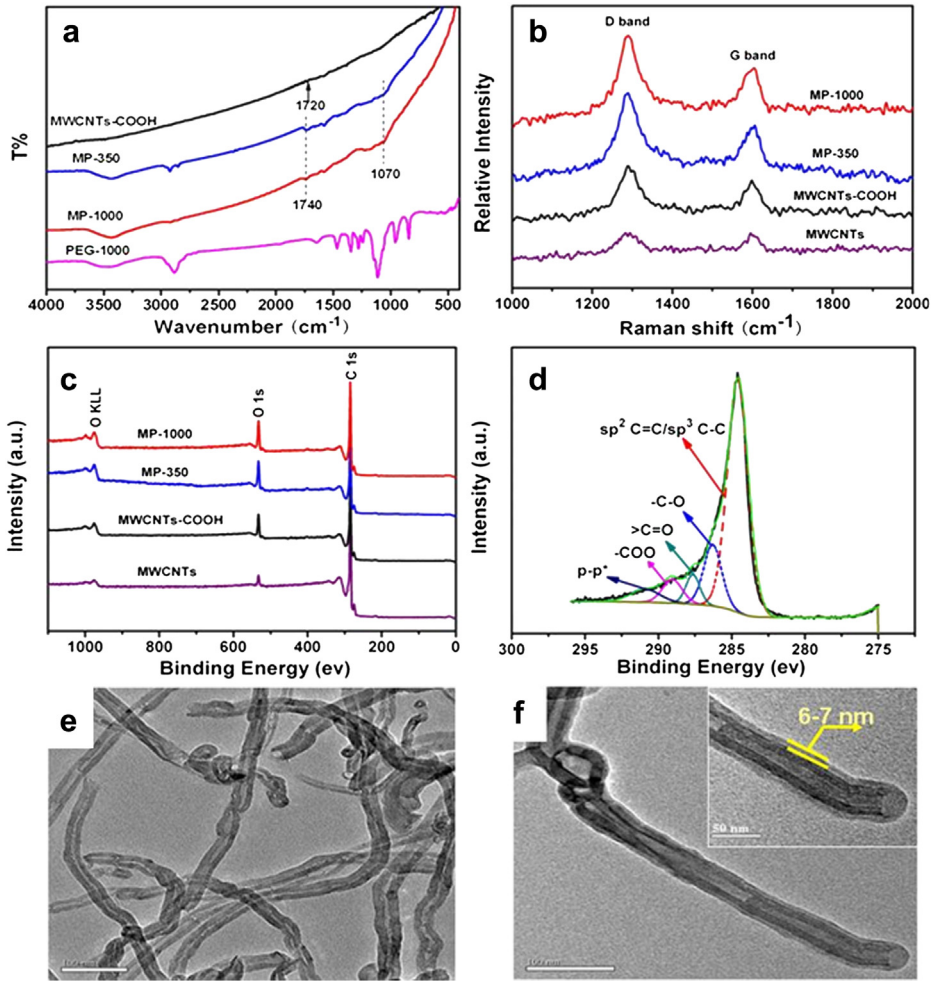

Fig. 1. Characterization of MP by (a) FTIR, (b) Raman and (c) Survey XPS spectra of MWCNTs, MWCNTs-COOH, MP-350 and MP-1000; (d) XPS C 1s peak deconvolution of MP-350; (e) TEM image of pristine MWCNTs; (f) TEM image of MP-1000.

(Fig. 1d) and MP-1000 (Fig. S2b) are compared to further understand this trend. The C 1s spectra have each been de-convoluted into five parts: peak 1 (~284.6 eV), sp^2 and sp^3 hybridized carbon; peak 2 (~286.3 eV), carbon in phenolic, alcohol, ether or C=N groups; peak 3 (~287.5 eV), carbon in carbonyl or quinine groups; peak 4 (~289.0 eV), carbon in carboxyl or ester groups; and peak 5 (~291.0 eV), $p-p^*$ transition [40]. The results of these five peaks for MWCNTs, MWCNTs-COOH, MP-350 and MP-1000 are given in Table S1 (see Supplementary materials). After the acid treatment and esterification, the content of sp^2/sp^3 carbon is clearly decreased, while the content of the functionalized carbon (including peak 2–peak 5) is increased. Hence, XPS provides strong evidence for the existence of grafted PEG on the surface of MWCNTs.

To prove the covalent linkage of PEG onto MWCNTs, the TEM technique was used to reveal the presence of PEG on the MWCNTs surface. As shown in Fig. 1e, MWCNTs are entangled with one another and have a clean and smooth surface in our observation. For the PEG-functionalized MWCNTs, a uniformly thin layer (6–7 nm) of a PEG shell surrounds the outer wall of every individual MWCNT along its length, thus forming so-called core–shell structures (Fig. 1f). But, the TEM image of the mixture of PEG and MWCNTs-COOH shows no polymer layer on the surface of MWCNTs (Fig. S3). The result proves that PEG is covalently grafted onto the MWCNTs. We also used TGA to determine the content of the grafted-PEG in the PEG-functionalized MWCNTs (as shown in Fig. S4a). The amounts of PEG 350 and 1000 grafts are approximately 30 wt.%.

3.2. Electrochemical performances

According to the effect of MWCNTs on the electrochemical performances of $LiFePO_4$, reported by Li et al. [15] and Xu et al. [41], the optimum MWCNTs content is suggested to be 5 wt.% in terms of cycle performance and efficient use of MWCNTs in balance. Therefore, to investigate the electrochemical performance of $LiFePO_4$-based cathodes for LIBs in our study, LFP/AB (5 wt.% and 20 wt.%), LFP/MWCNTs (5 wt.%) and LFP/MP (5 wt.%) were used to prepare the cathode candidates. Fig. 2a presents the first charge–discharge curves at 0.1C and 2.5–4.2 V. The cathode incorporating 5 wt.% of MWCNTs shows a similar 1st cycle discharge capacity (140 mAh g^{-1}) with the common cathode incorporating 20 wt.% of AB (see Fig. S5). However, the cathode composite with 5 wt.% of AB as a conductive additive exhibits only 135 mAh g^{-1} discharge capacity. Meanwhile, the discharge plateau potential of LFP/AB (5 wt.%) is apparently lower than the 20 wt.% AB case, which may originate from the cell polarization caused by the poor electric conductivity [42]. Interestingly and encouragingly, the discharge capacities of electrodes with MP as additive are higher than those of AB and MWCNTs, especially for the LFP/MP-350 composite cathode showing the highest discharge capacity of ~149 mAh g^{-1}, which is

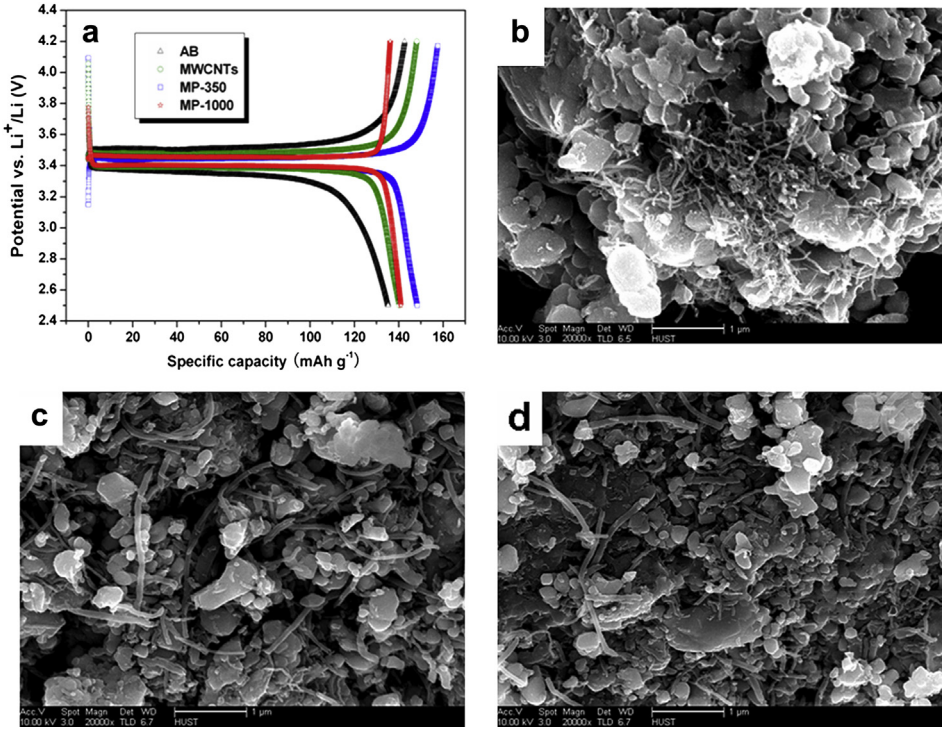

Fig. 2. (a) The first charge–discharge curves of $LiFePO_4$ cathodes with 5 wt.% of different conductive additives at 0.1C; (b) SEM image of $LiFePO_4$/MWCNTs (5 wt.%); (c) SEM image of $LiFePO_4$/MP-350 (5 wt.%); (d) SEM image of $LiFePO_4$/MP-1000 (5 wt.%). $LiClO_4$ was used to complex the MP in electrochemical measurements, and the molar ratio of the grafted-PEG to $LiClO_4$ corresponded to 8 mol of ethylene oxide for 1 mol of Li^+.

caused potentially by the different particle structure and size of these cathode materials.

We used SEM to compare the dispersion behaviors of MWCNTs and MP amongst $LiFePO_4$ particles. As shown in Fig. 2b, MWCNTs tend to agglomerate and are poorly dispersed in the active material. By contrast, PEG functionalized MWCNTs are uniformly dispersed in the host material since the PEG shell avoids tube–tube contacts and bundle formation (see Fig. 2c and d). Hence, MP can more easily connect $LiFePO_4$ particles to fabricate a continuous conductive network than pristine MWCNTs and used as novel conductive additives. Notably, the diameter of the tubes in the SEM images is larger than that of pristine MWCNTs, which further indicates the coating of a PEG shell on every single MWCNT. Also, from the XRD patterns, the crystal structures of LFP are not destroyed by the addition of different contents of PEG functionalized MWCNTs in the $LiFePO_4$ particles, as illustrated in Fig. S6.

The improved electrochemical performance has also been verified by the electrochemical impedance spectra (EIS). The intersection of the curve at high frequency to the real axis is related to the sum of ohmic resistance (R_s) of the Li^+ cells owing to the electrolyte, active materials, current collectors and separator [43]. The depressed semicircle in the medium-frequency region typically represents the double layer capacity and charge transfer resistance (R_{ct}) at the electrodes. The straight line at low frequency is attributed to the lithium ions diffusion in the cathode active materials. Fig. 3 shows the influence of different conductive additives on the EIS spectra of Li^+ cells with $LiFePO_4$ cathodes. It is clear that LFP/MWCNTs, LFP/MP-350 and LFP/MP-1000 cathodes with same content (5 wt.%) show lower R_{ct} (~160 Ω) than LFP/AB, indicating that LFP/MWCNTs and LFP/MP cathodes possess better reaction kinetics during electrochemical cycling than the LFP/AB cathodes. As discussed above, the effective conductive networks of LFP/MP cathodes therefore should be responsible for the improved cell performance.

As the kinetics of Li-ion diffusion through $LiFePO_4$-based cathodes plays an important role in the rate performance, the Li-ion diffusion coefficients (D_{Li+}) were calculated from Ref. [44]:

$$D_{Li^+} = \frac{R^2T^2}{2A^2n^4F^4C^2\sigma_w^2} \quad (1)$$

where R is universal gas constant (8.314 J mol^{-1} K^{-1}), T absolute temperature (298.15 K), A surface of the cathode, n number of electrons per molecule during oxidization, F the Faraday constant (96,500 C mol^{-1}), C molar concentration of Li ions, and σ_w Warburg

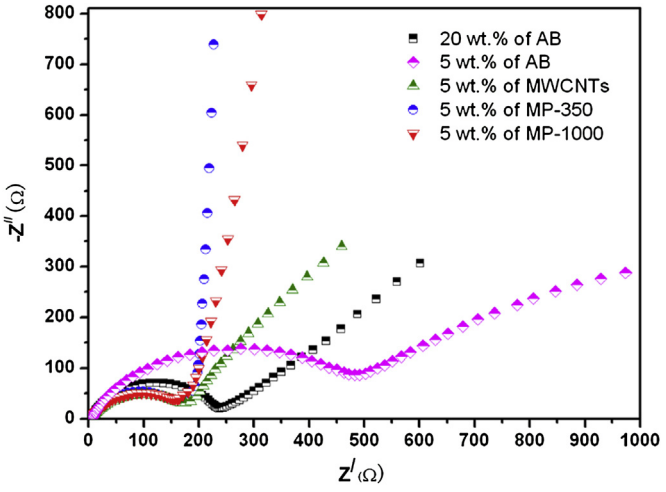

Fig. 3. EIS plots of LIBs with $LiFePO_4$ cathodes using different conductive additives.

Table 1
EIS parameters and Li-ion diffusion coefficients of the Li^+ cells with $LiFePO_4$-based cathodes in the presence of different additives.

Entry	Cathode additives	R_{ct} (Ω)	σ_w (Ω cm^2 $s^{-0.5}$)[a]	D_{Li+} (cm^2 s^{-1})[b]
1	20 wt.% of AB	241	97.5	3.2×10^{-14}
2	5 wt.% of AB	508	166.3	1.1×10^{-14}
3	5 wt.% of MWCNTs	156	76.5	5.2×10^{-14}
4	5 wt.% of MP-350	158	11.6	2.3×10^{-12}
5	5 wt.% of MP-1000	161	41.4	1.8×10^{-13}

[a] σ_w, the slope of the Z_{re} versus $\omega^{-1/2}$ plot.
[b] D_{Li+} is calculated from Eq. (1).

factor given by the slope of the plot of Z_{re} against the reciprocal root square of the lower angular frequencies ($\omega^{-1/2}$) (see Fig. S8).

To identify the improved electrochemical performance of PEG functionalized MWCNTs as $LiFePO_4$-based cathode additives, a series of D_{Li+} measurements in the presence of different additives were conducted, and the results are shown in Table 1. It is observed that D_{Li+} of LFP/AB (20 wt.%) is only 3.2×10^{-14} cm^2 s^{-1}, which may indicate deteriorated cell performance at high charge–discharge current density (see Fig. 4 later). Although the R_{ct} value of LFP/MWCNTs (5 wt.%) is much lower than those of LFP/AB (20 wt.%) and LFP/AB (5 wt.%), its D_{Li+} value is slightly higher (see Table 1). A possible explanation is that adding 5 wt.% MWCNTs into the cathode, and keeping other conditions unchanged, causes poor dispersion of MWCNTs in $LiFePO_4$ (see Fig. 2b), resulting in a relatively lower Li-ion diffusion. As shown by Yang et al. [19] in their $LiFePO_4$/graphene system, if the conductive additives are not well-dispersed in the $LiFePO_4$ matrix, graphene agglomeration will result in poor Li-ion diffusion, even if the electric conductivity of the active materials is improved to some degree. It should be pointed out that MWCNTs only is a kind of electrical conductor, which cannot solve the issue of low lithium ion diffusion in the $LiFePO_4$ cathode.

For LFP/MP (5 wt.%) samples, the Li^+ diffusion performance improved significantly when compared to LFP/AB and LFP/MWCNTs samples. In the case of LFP/MP-350 cathode, D_{Li+} is 2.3×10^{-12} cm^2 s^{-1}, which is ~2 orders of magnitude higher than LFP/AB (20 wt.%), as shown in Table 1. Such improvement can be explained as follows: PEG has good flexibility and high solubility for alkaline salts via interaction of its ether oxygen with cations [45]. It is widely accepted that the mixtures based on PEG that is doped by lithium salts have high ionic conductivity, high diffusion coefficient and, consequently, great potential for use as polymer electrolytes in LIBs. Therefore, in our study, PEG was applied as a coating on MWCNTs by a covalent method in order to obtain a mixed electron and lithium ion conductor so that both the electrical conductivity and Li-ion diffusion coefficient of $LiFePO_4$ cathode can be increased. Further, the lower the molecular weight of grafted PEG the higher is the D_{Li+} value (Table 1), probably due to the faster ion movement and transport in the MP cathode composite. Based on previous studies of molecular weight on ions transport in PEO-based polymer electrolytes [31,45], as the molecular weight of PEO increases, the free volume decreases and rearrangement of the polymer chains is hindered, resulting in slower ion movement and transport.

The carbon-based conductive additives are necessary for the cathode system, but excessive conductive carbon additives may decrease the energy density, induce side electrochemical reactions and increase the cost of the batteries [19]. As discussed above, the LFP cathode with MP-350 as the additive shows higher electrochemical performance than that of MP-1000 under the same experimental conditions. Hence, we used MP-350 as the conductive additive and examined its mass fraction effect on the LFP/MP electrode. Fig. S9 compares the initial charge–discharge curves of electrodes with different MP-350 content at 0.1C and the results are given in Table 2. The first discharge capacities are 143.3, 148.2, 152.3, 160, 150.6 and 150.9 mAh g^{-1}, respectively, for 3, 5, 8, 10, 15 and 20 wt.% of MP. Clearly, higher MP contents in the LFP/MPL electrode do not always give better cell performance. Similar results reported by other research groups [19,46] also support this finding here. The SEM images of LFP/MP with different contents of MP-350 (Fig. S10) show that, with 15 and 20 wt.%, MP is not well-dispersed within the $LiFePO_4$ particles, which is the reason for the low discharge capacity obtained. With 3 wt.% MP-350, the discharge capacity is 143.3 mAh g^{-1}, which is also low caused by the formation of a non-effective conductive network with insufficient MP (Fig. S10a). Even so, this value is still higher than the pristine MWCNTs (see Fig. 2a). From these results, we believe MP can serve as a practical conductive additive for $LiFePO_4$-based cathode materials.

As shown in Table 2, the electrode with 10 wt.% MP has the optimum charge–discharge performance. Cyclic voltammetry (CV) curves measured at 0.1 mV s^{-1} are given in Fig. S11. All samples

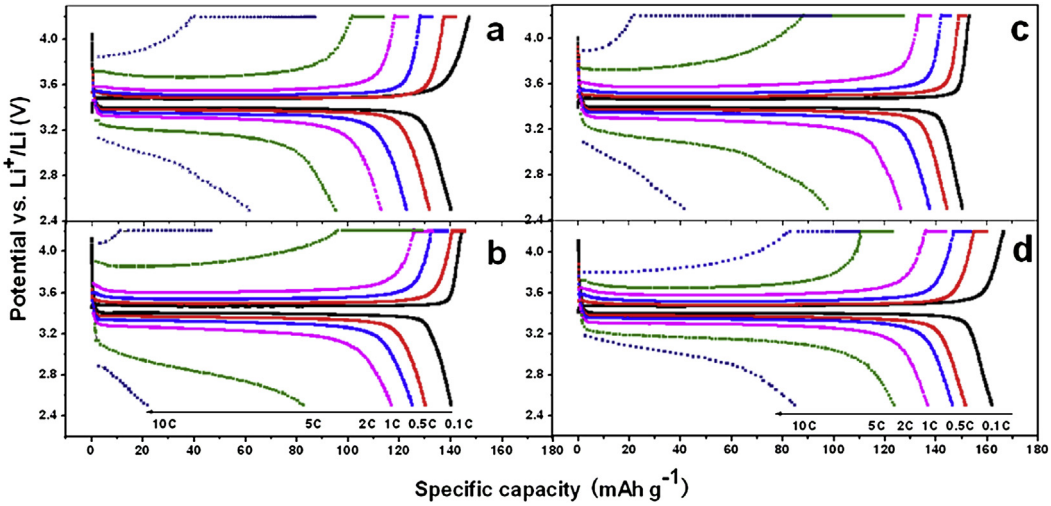

Fig. 4. Charge–discharge curves of (a) $LiFePO_4$/AB (20 wt.%), (b) $LiFePO_4$/AB (10 wt.%), (c) $LiFePO_4$/MWCNT (10 wt.%) and (d) $LiFePO_4$/MP-350 (10 wt.%) electrodes at different rates (identical charge and discharge rates were used).

Table 2
Electrochemical behaviors of $LiFePO_4$ with different mass fractions of MP-350.

Entry	Mass fraction of MP-350	Discharge capacity (mAh g^{-1})[a]	Peak potential difference (mV)[b]	I_O/I_R[c]
1	3 wt.%	143.3	448	1.40
2	5 wt.%	148.2	338	1.35
3	8 wt.%	152.3	341	1.27
4	10 wt.%	160.0	263	1.23
5	15 wt.%	150.6	376	1.40
6	20 wt.%	150.9	330	1.32

[a] The first charge–discharge experiments were carried out at 0.1C and 2.5–4.2 V.
[b] The CV parameters were obtained under 0.1 mV s^{-1} scan rate at the 3rd cycle.
[c] I_O/I_R is the current ratio of oxidation peak to reduction peak.

exhibit similar pair of peaks, consisting of an anodic and a cathodic peak, corresponding to the two-phase charge–discharge reaction of the Fe^{2+}/Fe^{3+} redox couple [17]. It is noted in Table 2 that the cell with 10 wt.% MP-350 additive displays the least potential difference between the symmetrical redox peaks (263 mV) and the lowest peak current ratio (I_O/I_R = 1.23), indicating the smallest electrode polarization and the best reversibility. These results support the effect of MP fraction on the LFP/MP electrode performance.

To satisfy the demands of high-power applications, a lithium-ion battery must deliver good performance at high charge–discharge current density. Fig. 4a–d presents the first cycle charge–discharge profiles obtained from coin-type half-cells containing LFP/AB (20 wt.%), LFP/AB (10 wt.%), LFP/MWCNTs (10 wt.%), and LFP/MP-350 (10 wt.%) cathodes with increasing C rates from 0.1C (=17 mA g^{-1}) to 10C between 2.5 and 4.2 V. All the cells were charged with constant current/constant voltage procedure. Although the discharge capacities of all tested electrodes were decreased gradually with the increasing current rate, the LFP/MP-350 (10 wt.%) electrode showed the most satisfactory discharge capacities and rate performance. For example, Fig. 4d illustrates its discharge capacities at 0.5C, 1C, 2C and 5C reach 151, 146, 136 and 123 mAh g^{-1}, respectively. Even at 10C, it still has a discharge capacity of 84 mAh g^{-1}, which is a 52% capacity retention compared to the capacity at 0.1C (161 mAh g^{-1}) at room temperature. This indicates an excellent rate performance of the LFP/MP composite cathode. By contrast, the discharge capacities for the LFP/AB (20 wt.%), LFP/AB (10 wt.%) and LFP/MWCNTs (10 wt.%) electrodes at 10C were rapidly reduced to 60, 22 and 46 mAh g^{-1}, respectively. On the subsequent rate cycling (Fig. 5a and b), the LFP/MP electrode still showed the best rate capacities compared with the LFP/AB and LFP/MWCNTs electrodes, especially at higher rates. Further, for all $LiFePO_4$-based cathodes studied, full capacity recoveries were observed at 0.1C cycling even after continuous cycling at 10C (Fig. 5a). This result indicates that there are no obvious structural damages for these four electrodes during the charge–discharge process.

The long-term cycle performances at low (0.1C) and high (5C) current densities were also characterized. As shown in Fig. 5b, the reversible discharge capacities for the LFP/MP electrode remained very stable and there was almost no capacity fading after 70 cycles at a 0.1C rate. However, a slight increase in discharge capacity occurred for the LFP/AB and LFP/MWCNTs electrodes during the first 3 cycles, which can be attributed to the slow electrolyte permeation into the electrodes or the formation of fissures on the carbon layer during cycling [16,47]. On subsequent cycling, the capacities for the LFP/AB and LFP/MWCNTs electrodes exhibited a slight fading but were more or less constant (Fig. 5b). Under the high current density of 850 mA g^{-1} (=5C), after 50 cycles, the LFP/MP electrode showed a capacity of 110 mAh g^{-1}, which is 89% capacity retention from the first cycle at a 5C (124 mAh g^{-1}), confirming the excellent cycling stability of LFP/MP. However, the reversible capacities for the LFP/AB (20 wt.%), LFP/AB (10 wt.%) and LFP/MWCNTs (10 wt.%) electrodes were only 70, 56 and 83 mAh g^{-1}, showing 73%, 68% and 81% capacity retention, respectively. We also evaluated the influence of temperature on the discharge capacities of LFP/AB (20 wt.%), LFP/AB (10 wt.%), LFP/MWCNTs (10 wt.%) and LFP/MP-350 (10 wt.%) electrode at 0.1C. As shown in Fig. 6, the discharge capacities of all the tested electrodes decreased with the decreasing of temperature. At the low temperature of 8 °C, the reversible discharge capacity of the LFP/MP-350 electrode was 138 mAh g^{-1} while the discharge capacities were 113, 111 and 126 mAh g^{-1} for the LFP/AB (20 wt.%), LFP/AB (10 wt.%), LFP/MWCNTs (10 wt.%) electrodes. Obviously, the LFP/MP-350 electrode exhibited a clear advantage with compared to the other electrodes at 8 °C. The contribution of the grafted PEG to the lithium ion diffusion and the dispersion of MWCNTs in the electrode may be responsible for this phenomenon because PEG was still in the amorphous liquid state. However, it is different from the situation at 0.1C at 8 °C and 25 °C that the LFP/MP-350 electrode showed only a slight capacity increase compared with the LFP/MWCNTs electrode at −20 °C. In addition to the low ionic conductivity of PEG at low temperature, the low Li^+ diffusivity in the $LiPF_6$-EC/DEC electrolyte system and the high charge-transfer resistance at the electrode/electrolyte interface also resulted in the limited electrode kinetics at relatively low temperature [4].

It is well known that the electrons and lithium ions should leave or reach active materials simultaneously for an ideal charge/discharge process [13,19]. According to our testing results in Table 3, the electrical conductivity for pure $LiFePO_4$ (LFP) (95% LFP and 5% PTFE binder) is only 7.83 × 10^{-6} S cm^{-1}, while the values of electrical conductivity for the cathode films with 20 wt.% AB and 10 wt.% MWCNTs are 0.196 and 0.355 S cm^{-1}, respectively. It is

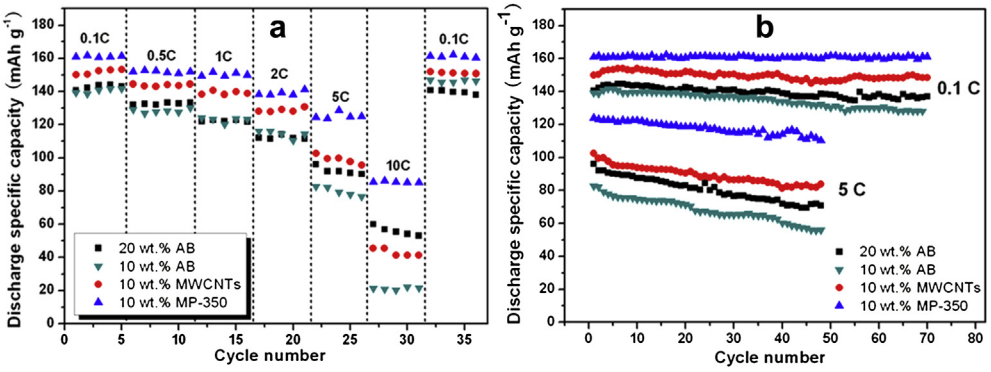

Fig. 5. (a) Rate capability and (b) cycling performance of the $LiFePO_4$ electrodes with different conductive additives.

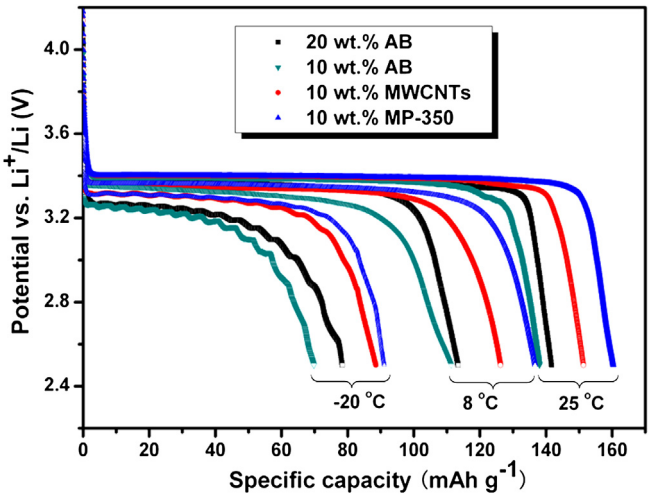

Fig. 6. Compare of the discharge curves of the $LiFePO_4$-based electrodes at 0.1C at different temperature. Specific charge current was 17 mA g^{-1} at 25 °C for all the cells.

noteworthy that for the LFP/MP-350 (10 wt.%) cathode film this value can reach as high as 0.380 S cm^{-1}. Hence, the excellent rate performance for the LFP/MP (10 wt.%) electrode, especially at high charge/discharge current densities (Fig. 4), can be partially attributed to its higher electrical conductivity. Besides, the effective conductive network provided by the MP incorporated into LFP can increase not only the electrons transportation but also the lithium ion diffusion rate in the cathode.

3.3. Thermal conductivity

To satisfy practical applications of LIBs, thermal safety of LIBs is a critical performance index. Thus, there are many investigations examining this aspect the cathodes. However, most [27,34,48] are focused on the cathode electrodes in the presence of electrolytes by performing differential scanning calorimetry (DSC) or TGA measurements. The thermal performance of cathodes is not truly reflected, which is caused by the interference of type and concentration of lithium salts, and solvents during testing. We only studied the thermal conductivity of the cathode itself without electrolyte and anode. The thermal conductivity values of the cathode films with different conductive additives are listed in Table 3. It can be seen that the thermal conductivity increases from 0.1601 W m^{-1} K^{-1} for the pure $LiFePO_4$ cathode film to 0.1741 and 0.1945 W m^{-1} K^{-1} for the LFP/AB (20 wt.%) and LFP/MWCNTs (10 wt.%) cathode films, respectively. Notably, for LFP/MP-350, the thermal conductivities of the films increase first with increasing MP-350 fraction and reach the highest value (0.264 W m^{-1} K^{-1}) at 10 wt.%, which is 1.65 times that of the pure $LiFePO_4$ cathode film.

Table 3
Electronic and thermal conductivities of different samples.

Entry	Cathode film	Electronic conductivity (S cm^{-1})[a]	Thermal conductivity (W m^{-1} K^{-1})[b]
1	LFP	7.83×10^{-6}	0.1601
2	LFP/AB (20 wt.%)	0.196	0.1741
3	LFP/MWCNTs (10 wt.%)	0.355	0.1945
4	LFP/MP-350 (5 wt.%)	0.018	0.2124
5	LFP/MP-350 (10 wt.%)	0.380	0.2643
6	LFP/MP-350 (15 wt.%)	0.486	0.2307
7	LFP/MP-350 (20 wt.%)	0.524	0.2327

[a] The electronic conductivities were conducted with four-probe method.
[b] The thermal conductivities were obtained using heat-pole method.

However, the thermal conductivity displays a descending trend with further increase in MP-350 fraction, possibly due to the poor dispersion of excessive MP-350 in the LFP matrix (see Figs. S10d and S10e). Obviously, the trends of electrical and thermal conductivities with increasing content of MP-350 in Table 3 are dissimilar. This is because heat is conducted in solids by two types of carriers-electrons and acoustic phonons, which is an ion-core vibrations in a crystal lattice [49]. It is well known that electron contribution to thermal runaway in conductors is dominant owing to the large concentrations of free electrons, while heat conduction in semiconductors is often determined by phonons [48,50]. Clearly, all the cathode films studied here are semiconductors based on the electrical conductivity results in Table 3. The poor dispersion of excess MP-350 in $LiFePO_4$ matrix may increase the phonons scattering probability, which deters heat conduction. Thus, combined with the results of electrochemical performances, the LFP/MP-350 system with 10 wt.% MP-350 exhibits the most satisfactory properties.

4. Conclusions

PEG grafted MWCNTs (MP) were synthesized and used as a novel conductive additive in $LiFePO_4$-based cathodes. The incorporation of MP into the $LiFePO_4$ matrix increased the electrochemical performance and Li-ion diffusion coefficient (D_{Li+}) of $LiFePO_4$ cathodes to varying degrees depending on the molecular weight of PEG grafted on the MWCNTs. With 5 wt.% conductive additives, the $LiFePO_4$/MP-350 cathodes showed higher discharge capacity (148.2 mAh g^{-1}, 0.1C) and D_{Li+} value (2.3×10^{-12} cm^2 s^{-1}) than the $LiFePO_4$/AB (135 mAh g^{-1}, 1.1×10^{-14} cm^2 s^{-1}) and $LiFePO_4$/MWCNTs (140 mAh g^{-1}, 5.2×10^{-14} cm^2 s^{-1}) cathodes due to the better dispersion of MP and the contribution of PEG on Li^+ diffusion. The reversible discharge capacities of the $LiFePO_4$/MP electrode at 8 °C and −20 °C were also enhanced when compared with the $LiFePO_4$/AB and $LiFePO_4$/MWCNTs electrodes. The improved rate capability and thermal conductivity on $LiFePO_4$-based cathodes by adding different MP-350 weight fractions showed that $LiFePO_4$/(10 wt.%) MP-350 possessed the optimum overall properties for high performance LIBs.

Acknowledgments

The authors sincerely thank the financial supports from Major International Joint Research Project (51210004) and Key Program (51035002) of the National Natural Science Foundation of China. We also thank the Analytical and Testing Center, Huazhong University of Science and Technology for access to XRD, TGA, SEM, and TEM measurements.

Appendix A. Supplementary data

Supplementary data related to this article can be found at http://dx.doi.org/10.1016/j.jpowsour.2013.07.091.

References

[1] L. Lu, X. Han, J. Li, J. Hua, M. Ouyang, J. Power Sources 226 (2013) 272–288.
[2] A.K. Padhi, K.S. Nanjundaswamy, J.B. Goodenough, J. Electrochem. Soc. 144 (1997) 1188–1194.
[3] A.K. Padhi, K.S. Nanjunclaswamy, C. Masquelier, S. Okada, J.B. Goodenough, J. Electrochem. Soc. 144 (1997) 1609–1613.
[4] L.X. Yuan, Z.H. Wang, W.X. Zhang, X.L. Hu, J.T. Chen, Y.H. Huang, J.B. Goodenough, Energy Environ. Sci. 4 (2011) 269–284.
[5] S.W. Oh, Z.D. Huang, B. Zhang, Y. Yu, Y.B. He, J.K. Kim, J. Mater. Chem. 22 (2012) 17215–17221.
[6] Y.N. Xu, S.Y. Chung, J.T. Bloking, Y.M. Chiang, W.Y. Ching, Electrochem. Solid-State Lett. 7 (2004) A131–A134.
[7] M. Armand, M. Gauthier, J.F. Magnan, N. Ravet, US Patent 0033360, 2004.

[8] Y. Lin, Y. Lin, T. Zhou, G. Zhao, Y. Huang, Z. Huang, J. Power Sources 226 (2013) 20–26.
[9] M. Inagaki, Carbon 50 (2012) 3247–3266.
[10] S.Y. Chung, J.T. Bloking, Y.M. Chiang, Nat. Mater. 1 (2002) 123–128.
[11] A. Yamada, S.C. Chung, K. Hinokuma, J. Electrochem. Soc. 148 (2001) A224–A229.
[12] S.W. Oh, Z.D. Huang, Y.B. He, B. Zhang, Y. Yang, Y.W. Mai, J.K. Kim, J. Mater. Chem. 22 (2012) 19643–19645.
[13] R. Dominko, M. Gaberšček, J. Drofenik, M. Bele, J. Jamnik, Electrochim. Acta 48 (2003) 3709–3716.
[14] K. Zaghib, J. Shim, A. Guerfi, P. Charest, K.A. Striebel, Electrochem. Solid-State Lett. 8 (2005) A207–A210.
[15] X. Li, F. Kang, X. Bai, W. Shen, Electrochem. Commun. 9 (2007) 663–666.
[16] O. Toprakci, H.A.K. Toprakci, L. Ji, G. Xu, Z. Lin, X. Zhang, ACS Appl. Mater. Interfaces 4 (2012) 1273–1280.
[17] X. Sun, J. Li, C. Shi, Z. Wang, E. Liu, C. He, X. Du, N. Zhao, J. Power Sources 220 (2012) 264–268.
[18] C.Y. Wu, G.S. Cao, H.M. Yu, J. Xie, X.B. Zhao, J. Phys. Chem. C 115 (2011) 23090–23095.
[19] F.Y. Su, C. You, Y.B. He, W. Lv, W. Cui, F. Jin, B. Li, Q.H. Yang, F. Kang, J. Mater. Chem. 20 (2010) 9644–9650.
[20] H. Kim, H. Kim, S.W. Kim, K.Y. Park, J. Kim, S. Jeon, K. Kang, Carbon 50 (2012) 1966–1971.
[21] X.M. Liu, Z. Huang, S. Oh, B. Zhang, P.C. Ma, M.M.F. Yuen, J.-K. Kim, Compos. Sci. Technol. 72 (2012) 121–144.
[22] J.N. Coleman, U. Khan, W.J. Blau, Y.K. Gun'ko, Carbon 44 (2006) 1624–1652.
[23] X.L. Xie, Y.W. Mai, X.P. Zhou, Mater. Sci. Eng. R 49 (2005) 89–112.
[24] Z.D. Huang, B. Zhang, Y.B. He, S.W. Oh, Y. Yu, J.K. Kim, J. Electrochem. Soc. 159 (2012) A2024–A2028.
[25] B. Zhang, Q.B. Zheng, Z.D. Huang, S.W. Oh, J.K. Kim, Carbon 49 (2011) 4524–4534.
[26] P. Kim, L. Shi, A. Majumdar, P.L. McEuen, Phys. Rev. Lett. 87 (2001) 215502.
[27] M.J. Ganter, R.A. DiLeo, C.M. Schauerman, R.E. Rogers, R.P. Raffaelle, B.J. Landi, Electrochim. Acta 56 (2011) 7272–7277.
[28] P.C. Ma, S.Y. Mo, B.Z. Tang, J.K. Kim, Carbon 48 (2010) 1824–1834.
[29] B. Zhao, H. Hu, A. Yu, D. Perea, R.C. Haddon, J. Am. Chem. Soc. 127 (2005) 8197–8203.
[30] E.B. Malarkey, R.C. Reyes, B. Zhao, R.C. Haddon, V. Parpura, Nano Lett. 8 (2008) 3538–3542.
[31] A. Panday, S. Mullin, E.D. Gomez, N. Wanakule, V.L. Chen, A. Hexemer, J. Pople, N.P. Balsara, Macromolecules 42 (2009).
[32] D.E. Fenton, J.M. Parker, P.V. Wright, Polymer 14 (1973) 589.
[33] H.W. Chen, F.C. Chang, Polymer 42 (2001) 9763–9769.
[34] K. Zaghib, J. Dubé, A. Dallaire, K. Galoustov, A. Guerfi, M. Ramanathan, A. Benmayza, J. Prakash, A. Mauger, C.M. Julien, J. Power Sources 219 (2012) 36–44.
[35] Q. Wang, P. Ping, X. Zhao, G. Chu, J. Sun, C. Chen, J. Power Sources 208 (2012) 210–224.
[36] X. Li, W. Guan, L. Hu, L. Huang, J. Funct. Mater. 35 (2004) 758–760.
[37] Y.K. Yang, X.L. Xie, J.G. Wu, Y.W. Mai, J. Polym. Sci. Part A: Polym. Chem. 44 (2006) 3869–3881.
[38] D.C. Sorescu, K.D. Jordan, P. Avouris, J. Phys. Chem. C 105 (2001) 11227–11232.
[39] Y.-X. Liu, Z.-J. Du, Y. Li, C. Zhang, C.-J. Li, X.-P. Yang, H.-Q. Li, J. Polym. Sci. Part A: Polym. Chem. 44 (2006) 6880–6887.
[40] T.I.T. Okpalugo, P. Papakonstantinou, H. Murphy, J. McLaughlin, N.M.D. Brown, Carbon 43 (2005) 153–161.
[41] J. Xu, G. Chen, X. Li, Mater. Chem. Phys. 118 (2009) 9–11.
[42] C. Ban, Z. Li, Z. Wu, M.J. Kirkham, L. Chen, Y.S. Jung, E.A. Payzant, Y. Yan, M.S. Whittingham, A.C. Dillon, Adv. Energy Mater. 1 (2011) 58–62.
[43] D. Andre, M. Meiler, K. Steiner, H. Walz, T. Soczka-Guth, D.U. Sauer, J. Power Sources 196 (2011) 5334–5341.
[44] Y. Cui, X. Zhao, R. Guo, Electrochim. Acta 55 (2010) 922–926.
[45] K. Hayamizu, E. Akiba, T. Bando, Y. Aihara, J. Chem. Phys. 117 (2002) 5929–5939.
[46] K.Q. Ding, L. Wang, J.J. Li, H.T. Jia, X.M. He, Int. J. Electrochem. Sci. 6 (2011) 6165–6176.
[47] R. Dominko, M. Bele, M. Gaberscek, M. Remskar, D. Hanzel, J.M. Goupil, S. Pejovnik, J. Jamnik, J. Power Sources 153 (2006) 274–280.
[48] S. Theil, M. Fleischhammer, P. Axmann, M. Wohlfahrt-Mehrens, J. Power Sources 222 (2013) 72–78.
[49] A.A. Balandin, Nat. Mater. 10 (2011) 569–581.
[50] A. Behrang, Master thesis, University of Montréal, Canada, 2012.